NANO LETTERS

pubs.acs.org/NanoLett Letter

Giant and Tunable Excitonic Optical Anisotropy in Single-Crystal Halide Perovskites

Georgy Ermolaev, Anatoly P. Pushkarev, Alexey Zhizhchenko, Aleksandr A. Kuchmizhak, Ivan Iorsh, Ivan Kruglov, Arslan Mazitov, Arthur Ishteev, Kamilla Konstantinova, Danila Saranin, Aleksandr Slavich, Dusan Stosic, Elena S. Zhukova, Gleb Tselikov, Aldo Di Carlo, Aleksey Arsenin, Kostya S. Novoselov, Sergey V. Makarov, and Valentyn S. Volkov*

Cite This: https://doi.org/10.1021/acs.nanolett.2c04792 Read Online

ACCESS | Metrics & More | Article Recommendations | Supporting Information

ABSTRACT: During the last years, giant optical anisotropy has demonstrated its paramount importance for light manipulation. In spite of recent advances in the field, the achievement of continuous tunability of optical anisotropy remains an outstanding challenge. Here, we present a solution to the problem through the chemical alteration of halogen atoms in single-crystal halide perovskites. As a result, we manage to continually modify the optical anisotropy by 0.14. We also discover that the halide perovskite can demonstrate optical anisotropy up to 0.6 in the visible range—the largest value among non-van der Waals materials. Moreover, our results reveal that this anisotropy could be in-plane and out-of-plane depending on perovskite shape—rectangular and square. As a practical demonstration, we have created perovskite anisotropic nanowaveguides and shown a significant impact of anisotropy on high-order guiding modes. These findings pave the way for halide perovskites as a next-generation platform for tunable anisotropic photonics.

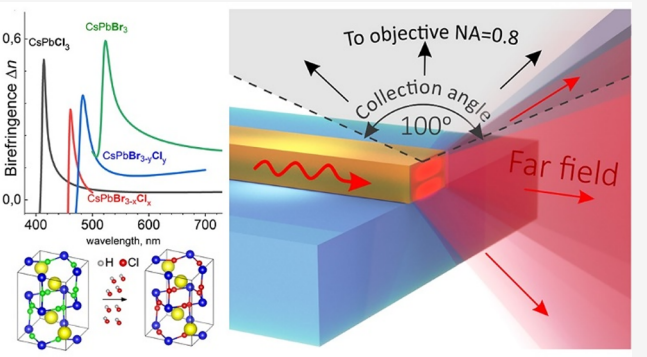

KEYWORDS: *halide perovskites, optical anisotropy, tunable optical properties, optical constants*

Optical anisotropy is one of the most useful and sought after effects for modern nanophotonics.[1] Aside from additional degree of freedom,[2] anisotropy enables novel physical effects and applications: extreme skin-depth guiding,[3] ultrastrong coupling,[4] polariton canalization,[5,6] achromatic waveplates,[7] switching nanolasers,[8] exciton-polariton transport,[3,9] lossless light confinement,[10] exceptional coupling,[11] topological singularities,[12] and ghost[13] and shear[14] polaritons, to name just a few. These breakthroughs have established a quest for anisotropic materials with giant and tunable birefringence Δn, which describes the speed of light difference between orthogonal directions.[15] The latest studies[3,16] have proposed the usage of van der Waals layered materials to tackle this problem since weak binding between atoms in one of the directions naturally leads to high birefringence. Additionally, layered structures are susceptible to atom intercalation, which is an efficient route for anisotropy manipulation.[17,18] Such methods of controlling anisotropy, however, do not allow for continuous adjustment, which results in a discrete number of material phases. Furthermore, the intercalation approach has been implemented only for the mid-infrared spectral range so far,[17,18] while the majority of photonic devices operate at visible frequencies.[12,19,20] As a result, tunable anisotropic optical response is in high demand.

In turn, halide perovskites is a family of materials where a variation of anions in the composition can dramatically change the band gap over the whole visible range.[21] In particular, the optical properties of perovskite composition $CsPbBr_{3-x}Cl_x$ can be easily tuned by exposure to HBr or HCl acids, even in gas phase.[21,22] More importantly, halide perovskites, for instance, $CsPbBr_3$, exhibit orthorhombic crystal structure (Figure 1a) at room temperature,[8,23,24] thus naturally having anisotropic optical response. Surprisingly, only recent research[7,8,25] has paid attention to anisotropy, while many others[26,27] continue to use the isotropic treatment. This inconsistency between works leads one to question why anisotropy can manifest itself only in limited cases. For this reason, accurate characterization of anisotropic dielectric tensors of halide perovskites is of paramount importance for advanced optics and perovskite applications.

Received: December 6, 2022
Revised: February 7, 2023

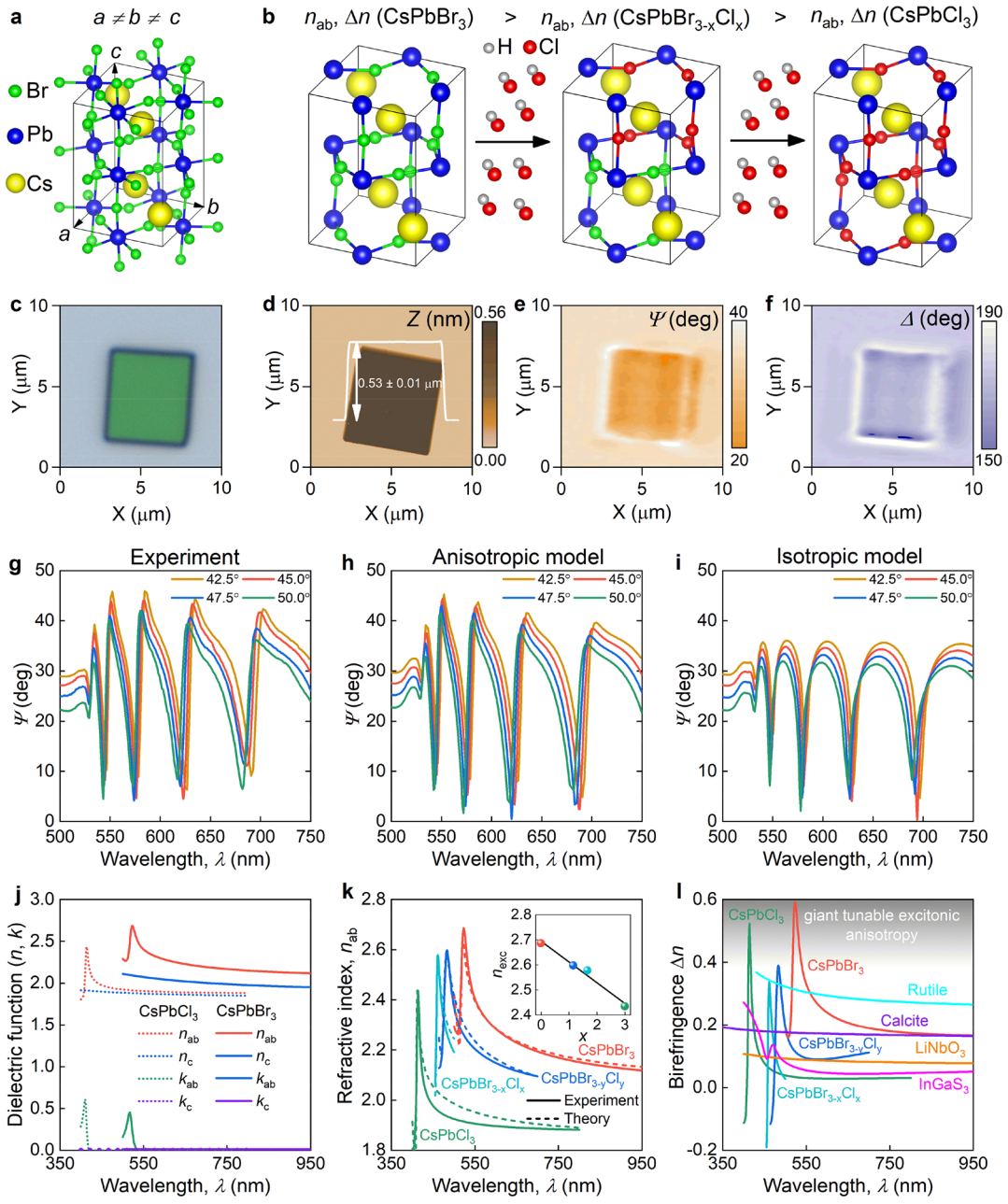

Figure 1. Tunability of halide perovskites dielectric tensor. (a) Orthorhombic crystal structure of $CsPbBr_3$. (b) Schematic illustration of chemical modification of halide perovskites. Representative (c) optical image, (d) atomic force microscopy topography and cross-sectional profile, and ellipsometric (e) Ψ and (f) Δ maps recorded at incident angle $\theta = 50°$ and $\lambda = 400$ nm of the $CsPbBr_{3-y}Cl_y$ microplate. (g) Experimental and theoretical ellipsometry spectra Ψ of $CsPbBr_3$ on the basis of (h) anisotropic and (i) isotropic model computations. (j) Anisotropic optical constants of $CsPbCl_3$ and $CsPbBr_3$. (k) Tunable refractive index of halide perovskite microplates for crystallographic *ab* plane. The inset shows the dependence of the refractive index at exciton resonance n_{exc} on stoichiometry number *x* of Cl atoms in $CsPbBr_{3-x}Cl_x$. (l) Tunable birefringence of halide perovskites in comparison with other anisotropic materials: rutile,[40] calcite,[39] $LiNbO_3$,[41] and $InGaS_3$.[38]

In this work, we resolve this challenge and demonstrate a broadband modification of the anisotropic optical properties of $CsPbBr_{3-x}Cl_x$ through variation of the chemical atomic composition. We have found that halide perovskite anisotropy is comparable to classical birefringent materials, such as rutile and calcite, at near-infrared wavelengths. Meanwhile, at exciton resonance, anisotropy reaches much higher values and exceeds all non-van der Waals materials. Additionally, our study shows that shape can determine the direction of the optical axis and, therefore, anisotropic tensors. As a practical demonstration, we present anisotropic waveguides based on $CsPbBr_3$. Remarkably, our results are applicable at all scales, nano, micro, and macro, unlike layered materials, which have to date demonstrated giant anisotropy only at the microscale. Moreover, halide perovskites possess countless benefits: low-cost fabrication,[28,29] high quantum yield of luminescence[30] and optical contrast,[31] strong excitonic response,[32,33] and wide composition diversity.[34,35] Therefore, the proposed tunable optical anisotropy in single-crystal $CsPbX_3$ offers an unprecedented platform for current and future perovskite nanophotonics and optoelectronics.

https://doi.org/10.1021/acs.nanolett.2c04792
Nano Lett. XXXX, XXX, XXX−XXX

The orthorhombic structure (a = 8.2563 Å, b = 8.2012 Å, c = 11.7308 Å) of halide perovskites, presented in Figure 1a, essentially results in different optical responses along orthogonal directions. These responses can be described by diagonal dielectric tensor diag(n_a,n_b,n_c), where n_a, n_b, and n_c are complex refractive indices along corresponding crystallographic basis (a,b,c). Provided that $a \approx b$ within 0.7% accuracy, and hence, $n_a \approx n_b = n_{ab}$, then halide perovskites are basically uniaxial crystals with dielectric tensor diag(n_{ab},n_{ab},n_c). Our polarized microtransmittance measurements in Supplementary Note 1 support this conclusion. To our surprise, polarized microtransmittance also showed that rectangular-shaped microplates have in-plane anisotropy, in contrast to square-shaped microplates that have out-of-plane anisotropy. The reason for this is because crystallographic axes determine the growth process of halide perovskites. Evidently, if in-plane crystallographic axes are the same ($a \approx b$), then the growth along both directions should be the same since there are no preferential directions. In that case, microplates result in a square shape. At the same time, crystallographic axes also define material polarizability and, therefore, refractive index. As a result, these square-shaped microplates have isotropic in-plane response and out-of-plane anisotropy. In the opposite case, where in-plane crystallographic axes are different, the growth process has a preferential direction that results in different optical responses. Therefore, rectangular-shaped microplates have in-plane anisotropy. Consequently, the shape of microplates immediately shows whether the microplate has in-plane (rectangular) or out-of-plane (square) anisotropy. This observation explains the inconsistency between anisotropic and isotropic responses of halide perovskite in recent works.[7,8,25−27]

In order to manipulate the crystal structure, we placed $CsPbBr_3$ microplates in HCl atmosphere (Supplementary Note 2). HCl reacts with the crystal by substituting Br atoms with Cl atoms, thereby resulting in an intermediate state $CsPbBr_{3-x}Cl_x$, as illustrated in Figure 1b. In this way, together with the crystal structure, we also controlled the whole dielectric tensor diag(n_{ab},n_{ab},n_c), which is described by two critical parameters: refractive index n_{ab} and birefringence $\Delta n = n_{ab} - n_c$. To investigate this effect, we leveraged imaging spectroscopic ellipsometry because it allows us detection of the optical signal even from microplates (Figure 1c). In order to boost the signal, we chose thick microplates (Figure 1d), which demonstrate Fabry−Perot resonances. They enhance the ellipsometer sensitivity to material anisotropy and produce characteristic asymmetric peaks in spectra.[3] Besides, we focused on microplates with out-of-plane anisotropy, which allow standard ellipsometry characterization. During the imaging ellipsometry, we also measured the maps of ellipsometric parameters Ψ (amplitude) and Δ (phase) (Figure 1e,f) from which we could deduce the local response of the microplates. As expected, the representative spectra in Figure 1g manifests numerous asymmetric oscillations in perfect agreement with anisotropic optical model, as shown in Figure 1h. At the same time, the isotropic optical model, plotted in Figure 1i, cannot describe the experimental data even qualitatively (Figure 1g). This demonstrates that halide perovskites, indeed, have high anisotropy in accordance with their orthorhombic structure.

For ellipsometry analysis, we noted high-quality Fabry−Perot resonances in Figure 1g, which indicated zero extinction coefficient k in the transparency region. At the same time, such resonances are strongly affected by the pronounced excitonic transition. By analogy to transition metal dichalcogenides,[3] we used the Tauc−Lorentz oscillator[36] and Cauchy model[3] for the crystallographic ab plane and c axis, respectively (Methods), in order to describe the dielectric function of halide perovskites. In particular, this description gave the ellipsometry spectra in Figure 1h, which is close to the actual data in Figure 1g. For additional verification, we also recorded the microtransmittance spectra, which coincides with the transfer matrix calculations, which are presented in Supplementary Note 3. Consequently, the Tauc−Lorentz and Cauchy models accurately characterize anisotropic optical response of halide perovskites.

On the basis of this description, we determined the modification of halide perovskite optical properties by HCl reaction. The mechanism relies on an anion exchange reaction that results in the formation of a shell saturated with chloride ions that diffuse in the volume of the crystal and produce a mixed-halide counterpart with evenly distributed anions.[37] Therefore, for microplates of the same thickness, chemical composition can be controlled by the time interval of exposure to HCl gas. For example, Figure 1j displays the results for $CsPbBr_3$ and $CsPbCl_3$, which defines the variation range of our tuning approach. Apart from absolute value change, it also controls the transparency region and can be used in switching photonic elements. Figure 1k,l demonstrates a monotonous refractive index and birefringence change with respect to the stoichiometric number x of Cl atoms in $CsPbBr_{3-x}Cl_x$. Interestingly, we can chemically tune perovskites' refractive index by 0.27 and anisotropy by 0.14. For instance, it allows us to cover anisotropic properties from $InGaS_3$[38] to calcite,[39] as seen from Figure 1l. At exciton resonance, however, anisotropy dramatically increases with values exceeding rutile birefringence (Figure 1l) and even reaches the optical anisotropy of hexagonal boron nitride (Supplementary Note 5). Hence, this giant anisotropic response originates from the exciton preferential direction along the crystallographic ab plane with respect to the c axis according to the Kramers−Kronig relation, similar to transition metal dichalcogenides.[3] It enables us to theoretically model optical properties of halide perovskites (see dashed lines in Figure 1k and Supplementary Note 5). Besides, our density functional theory calculations yield similar results for optical properties (Supplementary Note 6). Equally important, our tuning of Br with Cl occurs throughout the sample volume. Indeed, in the opposite case, we would have had to include the gradient of refractive index in our optical model in order to be able to fit ellipsometry data. Meanwhile, our data is perfectly described within a uniform refractive index model. Additional evidence of uniform substitution is a smooth linear change of the halide perovskites' refractive index, as shown in Figure 1k. Thus, our tuning of anisotropic dielectric tensors of halide perovskites relies on an exciton shift of the $CsPbBr_{3-x}Cl_x$ structure by altering the ratio of Br and Cl atoms.

It is worth noting that anisotropic properties of halide perovskites are not limited to microplates and can be found in macrocrystals, as well. For this purpose, we investigated $CsPbBr_3$ macroscopic samples (see the inset in Figure 2c), synthesized via antisolvent vapor-assisted crystallization (Methods).[42] The monocrystal nature of the $CsPbBr_3$ sample was confirmed by X-ray diffraction (XRD) measurements. The XRD spectrum, presented in Supplementary Note 7, which demonstrates four dominant diffraction peaks at 15.2°, 30.6°, 46.7°, and 63.9°, related to the (101), (202), (303), and (404)

https://doi.org/10.1021/acs.nanolett.2c04792
Nano Lett. XXXX, XXX, XXX−XXX

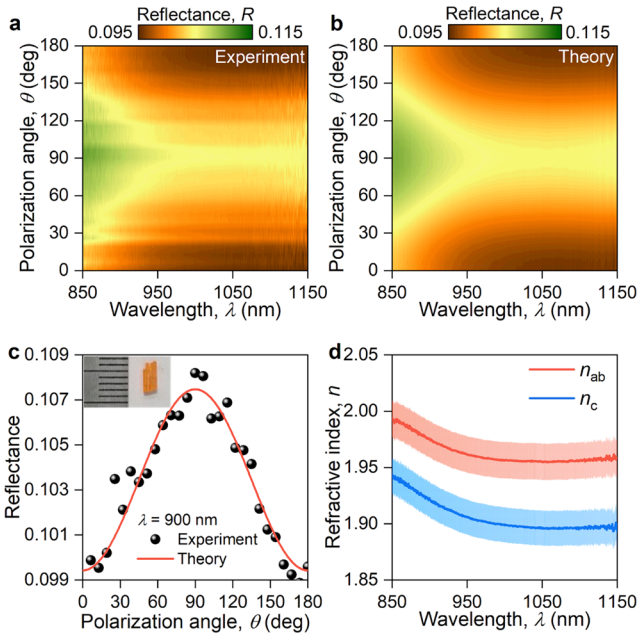

Figure 2. Anisotropic response of $CsPbBr_3$ macrocrystal. (a) Experimental and (b) theoretical polarized reflection of a $CsPbBr_3$ single crystal. (c) Representative reflection spectrum variations at λ = 900 nm with respect to polarization angles θ = 0° (180°) and 90° correspond to polarization along the crystallographic *c* axis and *ab* plane, respectively. The inset shows the photo of the investigated $CsPbBr_3$ crystal. (d) Anisotropic optical properties of $CsPbBr_3$ macrocrystal obtained from the fitting of panel (a). Error bars in the graph are taken from fitting errors.

plane of the orthorhombic $CsPbBr_3$ perovskite with the *Pnma* space group.

For anisotropy investigation, we recorded polarized reflection, plotted in Figure 1a. It immediately indicates that our samples are anisotropic because of a clear reflectance sinusoidal behavior upon polarization. To get the qualitative description, we fitted the experimental spectra (Figure 1a):

$$R(\lambda, \theta) = \left(\frac{n_c(\lambda) - 1}{n_c(\lambda) + 1}\right)^2 \cos^2(\theta) + \left(\frac{n_{ab}(\lambda) - 1}{n_{ab}(\lambda) + 1}\right)^2 \sin^2(\theta) \quad (1)$$

where $R(\lambda, \theta)$ is the reflection coefficient at a given wavelength λ and polarization angle θ, and $n_{ab}(\lambda)$ and $n_c(\lambda)$ are wavelength-dispersive refractive indices of $CsPbBr_3$. Figure 2b shows the resulting theoretical reflectance and Figure 2c demonstrates an exemplified fitting of polarized transmittance at given wavelength λ = 900 nm. Similar to microplates, large monocrystal $CsPbBr_3$ exhibits a higher refractive index along the crystallographic *ab* plane n_{ab} than along crystallographic *c* axis n_c, as seen from Figure 2d. As a result, the anisotropic properties of halide perovskites can be implemented not only in nanophotonics but also in bulky optical devices, such as waveplates or polarizers.

Optical anisotropy is also critical for nanophotonic designs[43] where geometrical sizes move to subwavelength scales. Besides, anisotropy in perovskites can be leveraged in a variety of waveguide configurations[44] for numerous applications, including phase matching for nonlinear processes[45] and tunable Dyakonov surface waves.[46] In order to show the strong effect of anisotropy at nanoscale, we considered a $CsPbBr_3$ nanowaveguide (NW) with a diffraction grating on its top face. Depending on its period, such grating allows for an efficient angle-dependent coupling of the incident light into propagating modes of NW at a certain wavelength λ_{in} (Figure 3a). Solution-synthesized monocrystalline $CsPbBr_3$ nanowires (protocol is available elsewhere[47]) on an indium tin oxide (ITO) substrate were used as a base for such NWs. Structural analysis on the synthesized nanowires confirmed that their crystallographic axes were oriented perpendicularly to those in the abovementioned $CsPbBr_3$ microplate (see Supplementary Note 8), i.e., n_c was oriented along the *z* axis and $n_a = n_b$ were in the *x*−*y* plane. Femptosecond laser projection lithography was further applied to imprint surface grating on the top face of the $CsPbBr_3$ nanowire (for details, see Methods).[47] An example of a 20 μm length nanowire with a rectangular cross-section (1 × 0.47 μm^2) containing a laser-printed 260 nm period surface grating on the top face is shown in Figure 3b. Noteworthy, the laser patterning does not cause any detectable changes of either crystallinity or photoluminescence quantum yield of the nanowire (see Supplementary Note 9).

We further analyzed the spectrum of the $CsPbBr_3$ NW modes that were excited by a collimated linearly polarized beam from a supercontinuum generator at different angles of incidence θ and out-coupled the NW from one of its facets (for details, see Supplementary Note 10). This allowed us to reconstruct the dispersion of the main waveguiding modes supported by the NW. The measurement results are summarized in Figure 3c, which reveal several bright branches that can be attributed to certain modes supported by the $CsPbBr_3$ nanowire. Theoretical mode analysis for an infinitely long $CsPbBr_3$ NW with a rectangular-shaped cross-section (Figure 3c,d) was carried out to calculate the dispersion characteristics of the waveguiding modes. We considered the first-order diffraction condition $\Lambda(\lambda_{in}) = \lambda_{in}/[n_{eff}(\lambda_{in}) - \sin\theta]$ and anisotropic refractive index of the $CsPbBr_3$ (Figure 1j). The calculation results for the strongest hybrid electromagnetic waveguide $(EH)_{00}$-, EH_{10}-, and EH_{20}-modes (EH indicates that transverse magnetic component dominates transverse electric component) are plotted in the Figure 3c as solid curves, which also demonstrate a perfect matching of the calculated and the experimentally measured dispersion curves in the case of the EH_{10}- and EH_{20}-modes. Such matching could not be achieved with any isotropic refractive index of the $CsPbBr_3$ (dashed curves in Figure 3c), thereby indicating strong optical anisotropy of the NW. It should be noted, the dispersion curve corresponding to the fundamental EH_{00}-mode is also marked in Figure 3c. However, this mode cannot be experimentally detected because of weaker (with respect to EH_{10}- and EH_{20}-modes) excitation efficiency and the mismatch between its out-coupling directivity and the collection angle of the microscope objective (≈100°, NA = 0.8) used in the experimental setup (Figure 3d; for details, see Supplementary Notes 10 and 11).

In summary, we measured the refractive index tensor of $CsPbBr_3$ for the first time and demonstrated its anisotropic optical response at all scales from nano to macro. This anisotropy originates from crystal low symmetry and selective direction of the exciton formation. Surprisingly, $CsPbBr_3$ exhibits the highest birefringence (up to 0.6) among non-van der Waals materials. Apart from giant anisotropy, this birefringence can be modified by chemical substitution of Br with Cl atoms. As a result, anisotropy can take any value from $CsPbBr_3$ to $CsPbCl_3$ dielectric tensor since chemical reaction results in intermediate state $CsPbBr_{3-x}Cl_x$ with continually

https://doi.org/10.1021/acs.nanolett.2c04792
Nano Lett. XXXX, XXX, XXX−XXX

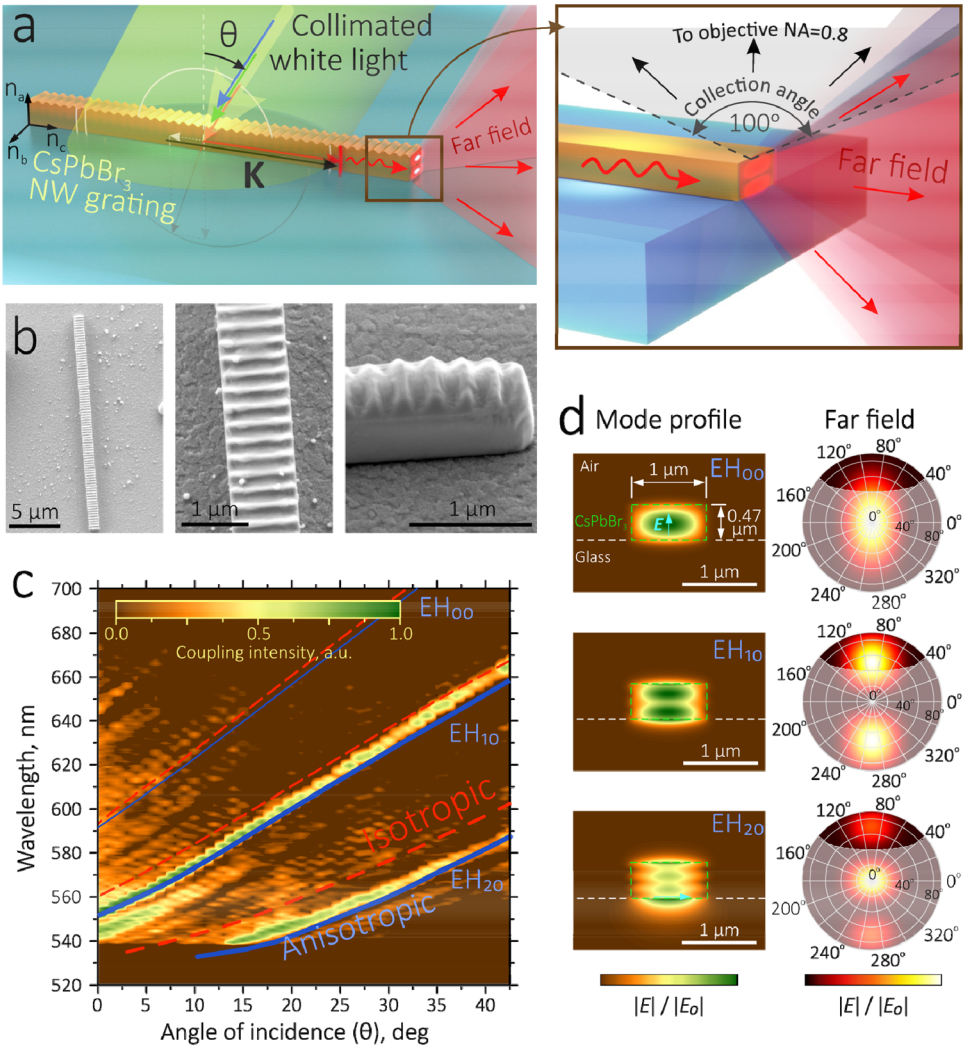

Figure 3. Optical anisotropy in $CsPbBr_3$ nanowaveguide. (a) Schematic illustration of the angled excitation of the $CsPbBr_3$ perovskite nanowaveguide, as well as out-coupling of the modes. (b) SEM images of the perovskite nanowaveguide with a 260 nm period nanograting. (c) Measured and calculated dispersion law for the first three (EH_{00}, EH_{10} and EH_{20}) waveguide modes supported by the perovskite nanowaveguide. Calculations were carried out considering both the anisotropic (solid curves) and isotropic (dashed curves) nanowaveguide. (d) Calculated intensity profiles and far-field outcoupling directivities for the considered waveguide modes.

tuned Br and Cl concentrations. Finally, halide perovskite can change it optical axis, resulting in in-plane and out-of-plane anisotropy, depending on the shape. Hence, halide perovskites greatly expand the library of anisotropic materials and present novel opportunities for tunable anisotropic nanophotonics.

METHODS

Ellipsometry and Microtransmittance Measurements. For the ellipsometry measurements, we used an Accurion nanofilm_ep4 ellipsometer in rotating compensator mode with focus scan to ensure that the sample surface would be in focus. Measurements were done in a 1 nm step and at several incident angles (42.5°, 45°, 47.5°, 50°).

Microtransmittance Measurements. Transmittance was recorded on an Accurion nanofilm_ep4 ellipsometer at 90° position of input and output branch. First, we measured the camera signal, corresponding to each sample, and then the reference and background signals from the same area. Transmittance was calculated as a ratio of sample to reference signals with subtracted background contribution.

Reflectance Measurements. The reflectance spectra were obtained using a Hyperion 2000 microscope incorporated into a Bruker Vertex 80 V spectrometer. For reference, we used a gold mirror.

Optical Microscopy. The images of halide perovskite microplates were captured by an optical microscope (Nikon LV150L) with a digital camera DS-Fi3.

Atomic Force Microscopy. AFM measurements were performed in air by a commercial AFM (NT-MDT N'tegra II, Moscow, Russia; www.ntmdt-si.ru) The topography data was registered in semicontact mode by Nova_PX acquisition software integrated with the AFM instrument using HA_NC cantilevers with tip-tapping resonant frequency around 145 kHz. The image processing and quantitative analysis were done using Gwyddion software (www.gwyddion.net).

Synthesis of Halide Perovskite Microwires and Microplates. Perovskite microwires on glass and ITO substrates were synthesized by using a protocol similar to the previously reported one.[47] Both 110 mg of $PbBr_2$ and 62 mg of CsBr were mixed and dissolved in 3 mL of anhydrous dimethyl sulfoxide (DMSO) inside a N_2-filled glovebox. Two

https://doi.org/10.1021/acs.nanolett.2c04792
Nano Lett. XXXX, XXX, XXX−XXX

μL of the prepared solution was drop casted on an ITO substrate at ambient conditions. Then, the substrate was sealed in a Petri dish preheated up to 60 °C containing 200 μL of liquid 2-propanol−water azeotropic mixture (85%). The droplet was dried in the presence of azeotropic vapor at 60 °C for 5 min. As a result, ensembles of separate microwires were formed on the substrate.

Amorphous Al_2O_3 substrate with island morphology was fabricated according to the protocol reported elsewhere.[48] Perovskite microplates on the substrate were synthesized by utilizing the same precursor solution in which 20 μL of deionized water was added (Supplementary Figure 5). The protocol is the same to the abovementioned.

Synthesis of Halide Perovskite Crystal. Perovskite monocrystals were synthesized via antisolvent vapor-assisted crystallization (AVC), as described by Dirin and coauthors.[42] Bromide precursors CsBr and $PbBr_2$ were dissolved in dipolar aprotic solvent with an excess of Cs component. Into 1 mL of dimethyl sulfoxide (DMSO) was dissolved 56.82 mg of CsBr and 146.80 mg of $PbBr_2$. The solution was prepared under argon atmosphere and was stirred overnight at room temperature. Next, 0.3 mL water was added into the solution. The solution was filtered through PTFE (polytetrafluoroethylene) 0.45 μm syringe filters before the growth process.

Antisolvent mixture was made by mixing ethanol and water in a 1:6 volume ratio. The growth kit was set as a Russian nesting doll: perovskite precursor solution in a small vial with no cap was placed inside bigger antisolvent vial. We observed that the growth rate and crystal quality depended on the gas−liquid interface of solvent and antisolvent. The variety of vials size ratio were tested. The best result was achieved with 4 and 20 mL vials. The setup was placed on a marble antivibration table at room temperature (295 K) until crystals reached the diameter of the small vial. The crystals had a plate shape, the dimension was 9 mm in length, 2 mm in width, and 1 mm tall.

X-ray Diffraction. To confirm the monocrystal nature of the grown $CsPbBr_3$ samples, we performed the XRD analysis with Cu source. The XRD spectra of bulk monocrystals (Supplementary Note 3) show four dominant diffraction peaks at 15.2°, 30.6°, 46.7°, and 63.9°, which can be related to the 101, 202, 303, and 404 planes of the orthorhombic $CsPbBr_3$ perovskite with *Pnma* space group.[49]

Investigation of the structural properties for $CsPbBr_3$ monocrystals XRD patterns were recorded on a Bruker D8 Discover X-ray diffractometer with Cu Kα radiation (1.54184 Å).

The XRD patterns of microwire (Supplementary Figure 8a) and microplate (Supplementary Figure 4a) ensembles were recorded in the $\theta-\theta$ geometry on an XRD-7000 diffractometer (Shimadzu) equipped with a 2 kW rotating Cu anode tube, beam collimator, and optical microscope. The X-ray beam was collimated to the 100 μm diameter spot, and the measurements were carried out in the scan range 2θ = 10−60° with 0.002° precision. It was established microwires and microplates possess orthorhombic structure and crystallize in two different space groups: *Pbnm* and *Pnma*, respectively.

Transmission Electron Microscopy. TEM, HRTEM, SAED, and FFT images (Figures S8b−d and S9b,c) were obtained on an FEI Tecnai F20 X-TWIN transmission electron microscope with a field emission gun. Sample measurements were carried out using the bright-field regime, the acceleration tension set for 200 kV, and images recorded using a Gatan Orius CCD camera. Perovskite crystals were synthesized on TEM grids according to the protocols employed for the production of microwires and microplates. The images confirm a monocrystalline structure of perovskite crystals (for details, see Supplementary Note 1).

Grating Imprinting on the Anisotropic $CsPbBr_3$ Nanowaveguide. Direct femtosecond laser (180 fs pulse duration, 515 nm wavelength) projection lithography was used to imprint the surface grating on the top face of the $CsPbBr_3$ nanowire. The output laser beam was first shaped into a flat-top stripe-shape beam using an aperture drilled in aluminum foil. The generated intensity profile was then projected with magnification from the aperture plane to the microscope objective focal plane using a 4*f*-optical system yielding generation of a 400 nm width and 5 μm length laser stripe with uniform intensity distribution and with fluence around 50 mJ cm^{-2}. A single-pulse single-trench laser patterning regime of the $CsPbBr_3$ nanowire with such a stripe-shaped beam at constant scanning speed (on μm/s scale) and pulse repetition rate (on Hz scale) was used to imprint the nanograting with the desired period and depth up to 30 nm. The quality of the nanowires nanopatterning was monitored by optical microscopy in situ. Additional details can be found elsewhere.[27]

Optical Modeling. Intensity profiles of the certain waveguide modes supported by the $CsPbBr_3$ nanowire with a rectangular cross-section, as well as out-coupling directivities of these modes, were calculated using commercial Lumerical Mode Solutions software package.

■ ASSOCIATED CONTENT

Supporting Information

The Supporting Information is available free of charge at https://pubs.acs.org/doi/10.1021/acs.nanolett.2c04792.

> Details on the dependence of optical axis direction on perovskite microplate shape and experimental methods for the synthesis of $CsPbBr_3$ and $CsPb(Cl,Br)_3$ microplates, microtransmittance validation of ellipsometry results for halide perovskite optical properties, comparison of halide perovskite anisotropy with other anisotropic materials, phenomenological description of halide perovskite optical responses, density functional theory of $CsPbBr_3$ optical constants, XRD spectrum of $CsPbBr_3$ macrocrystal, structural characterization of $CsPbBr_3$ microwires, Raman spectra of the as-synthesized and laser-patterned $CsPbBr_3$ nanowire, analysis of the mode excitation efficiency, and measurement of the dispersion characteristics of the waveguide modes supported by $CsPbBr_3$ nanowire; Supplementary Figures 1−17; Supplementary Table 1 (PDF)

■ AUTHOR INFORMATION

Corresponding Author

Valentyn S. Volkov − *Emerging Technologies Research Center, XPANCEO, Dubai 00000, United Arab Emirates;* orcid.org/0000-0001-8994-7812; Email: vsv@xpanceo.com

Authors

Georgy Ermolaev − *Emerging Technologies Research Center, XPANCEO, Dubai 00000, United Arab Emirates; Center for Photonics and 2D Materials, Moscow Institute of Physics and Technology, Dolgoprudny 141700, Russia;* orcid.org/0000-0002-0895-818X

https://doi.org/10.1021/acs.nanolett.2c04792
Nano Lett. XXXX, XXX, XXX−XXX

Anatoly P. Pushkarev − *ITMO University, School of Physics and Engineering, St. Petersburg 197101, Russia;* orcid.org/0000-0002-1793-6812
Alexey Zhizhchenko − *Far Eastern Federal University, Vladivostok 690091, Russia; Institute of Automation and Control Processes, Far Eastern Branch, Russian Academy of Science, Vladivostok 690041, Russia*
Aleksandr A. Kuchmizhak − *Far Eastern Federal University, Vladivostok 690091, Russia; Institute of Automation and Control Processes, Far Eastern Branch, Russian Academy of Science, Vladivostok 690041, Russia;* orcid.org/0000-0002-5376-5555
Ivan Iorsh − *ITMO University, School of Physics and Engineering, St. Petersburg 197101, Russia;* orcid.org/0000-0003-4992-6122
Ivan Kruglov − *Emerging Technologies Research Center, XPANCEO, Dubai 00000, United Arab Emirates; Center for Photonics and 2D Materials, Moscow Institute of Physics and Technology, Dolgoprudny 141700, Russia; Dukhov Research Institute of Automatics (VNIIA), Moscow 127055, Russia*
Arslan Mazitov − *Center for Photonics and 2D Materials, Moscow Institute of Physics and Technology, Dolgoprudny 141700, Russia; Dukhov Research Institute of Automatics (VNIIA), Moscow 127055, Russia*
Arthur Ishteev − *LASE − Laboratory of Advanced Solar Energy, NUST MISiS, Moscow 119049, Russia; N.N. Semenov Federal Research Center for Chemical Physics, Russian Academy of Sciences, Moscow 119991, Russia*
Kamilla Konstantinova − *LASE − Laboratory of Advanced Solar Energy, NUST MISiS, Moscow 119049, Russia; Research and Practical Clinical Center for Diagnostics and Telemedicine Technologies of the Moscow Health Care Department, Moscow 127051, Russia*
Danila Saranin − *LASE − Laboratory of Advanced Solar Energy, NUST MISiS, Moscow 119049, Russia*
Aleksandr Slavich − *Center for Photonics and 2D Materials, Moscow Institute of Physics and Technology, Dolgoprudny 141700, Russia*
Dusan Stosic − *Center for Photonics and 2D Materials, Moscow Institute of Physics and Technology, Dolgoprudny 141700, Russia*
Elena S. Zhukova − *Center for Photonics and 2D Materials, Moscow Institute of Physics and Technology, Dolgoprudny 141700, Russia;* orcid.org/0000-0002-5482-9477
Gleb Tselikov − *Emerging Technologies Research Center, XPANCEO, Dubai 00000, United Arab Emirates; Center for Photonics and 2D Materials, Moscow Institute of Physics and Technology, Dolgoprudny 141700, Russia*
Aldo Di Carlo − *LASE − Laboratory of Advanced Solar Energy, NUST MISiS, Moscow 119049, Russia; CHOSE − Centre of Hybrid and Organic Solar Energy, Department of Electronics Engineering, Rome 00133, Italy*
Aleksey Arsenin − *Emerging Technologies Research Center, XPANCEO, Dubai 00000, United Arab Emirates; Center for Photonics and 2D Materials, Moscow Institute of Physics and Technology, Dolgoprudny 141700, Russia; Laboratory of Advanced Functional Materials, Yerevan State University, Yerevan 0025, Armenia*
Kostya S. Novoselov − *National Graphene Institute (NGI), University of Manchester, Manchester M13 9PL, United Kingdom; Institute for Functional Intelligent Materials, National University of Singapore, 117544, Singapore; Chongqing 2D Materials Institute, Chongqing 400714, China*
Sergey V. Makarov − *ITMO University, School of Physics and Engineering, St. Petersburg 197101, Russia; Qingdao Innovation and Development Center, Harbin Engineering University, Qingdao, Shandong 266000, China;* orcid.org/0000-0002-9257-6183

Complete contact information is available at: https://pubs.acs.org/10.1021/acs.nanolett.2c04792

Author Contributions

A.P.P., A.D.C., A.A., K.S.N., S.V.M., and V.S.V. suggested and directed the project. G.E., A.P.P., A.Z., A.A.K., A.S., D.Stosic, E.S.Z., and G.T. performed the measurements and analyzed data. A.P.P., A.I., K.K., and D.Saranin designed and fabricated the samples. I.K., A.M., and I.I. provided theoretical support. G.E., A.P.P., A.Z., A.A.K., I.I., I.K., A.M., A.I., D.Saranin, G.T., A.D.C., A.A., K.S.N., S.V.M., and V.S.V. contributed to the interpretation of the experimental results. G.E., A.P.P., and S.V.M. wrote the original draft. G.E., A.P.P., A.I., I.I., A.D.C., A.A., K.S.N., S.V.M., and V.S.V. reviewed and edited the paper. All authors contributed to the discussions and commented on the paper.

Notes

The authors declare no competing financial interest.

■ ACKNOWLEDGMENTS

A.S., D.Stosic, G.T., and A.A. acknowledge the financial support from the Ministry of Science and Higher Education of the Russian Federation (Agreement No. 075-15-2021-606) for microtransmittance and Raman measurements. G.E., I.K., and A.M. gratefully acknowledge the financial support from of the Russian Science Foundation (No. 22-19-00738) for ellipsometry measurements and first-principle calculations. A.I., K.K., and D.Saranin gratefully acknowledge the financial support from the Russian Science Foundation (No. 21-19-00853) for the synthesis of the halide perovskite crystal. S.V.M. and A.P.P. acknowledge the Ministry of Science and Higher Education of the Russian Federation (Agreement No. 075-15-2021-589) for the fabrication and characterization of perovskite nanowaveguides. K.S.N. is grateful to the Ministry of Education, Singapore (Research Center of Excellence award to the Institute for Functional Intelligent Materials I-FIM, project No. EDUNC-33-18-279-V12) and to the Royal Society (UK, grant number RSRP\R\190000) for support.

■ REFERENCES

(1) He, M.; et al. Anisotropy and Modal Hybridization in Infrared Nanophotonics Using Low-Symmetry Materials. *ACS Photonics* **2022**, *9*, 1078−1095.
(2) Jahani, S.; Jacob, Z. All-dielectric metamaterials. *Nat. Nanotechnol.* **2016**, *11*, 23−36.
(3) Ermolaev, G. A.; Grudinin, D. V.; Stebunov, Y. V.; Voronin, K. V.; Kravets, V. G.; Duan, J.; Mazitov, A. B.; Tselikov, G. I.; Bylinkin, A.; Yakubovsky, D. I.; et al. Giant optical anisotropy in transition metal dichalcogenides for next-generation photonics. *Nat. Commun.* **2021**, *12*, 854.
(4) Bylinkin, A.; et al. Real-space observation of vibrational strong coupling between propagating phonon polaritons and organic molecules. *Nat. Photonics* **2021**, *15*, 197−202.
(5) Duan, J.; et al. Twisted Nano-Optics: Manipulating Light at the Nanoscale with Twisted Phonon Polaritonic Slabs. *Nano Lett.* **2020**, *20*, 5323−5329.

(6) Hu, G.; et al. Topological polaritons and photonic magic angles in twisted α-MoO_3 bilayers. *Nature* **2020**, *582*, 209−213.
(7) Chen, X.; et al. Solution-processed inorganic perovskite crystals as achromatic quarter-wave plates. *Nat. Photonics* **2021**, *15*, 813−816.
(8) Du, W.; et al. All Optical Switching through Anistropic Gain of $CsPbBr_3$ Single Crystal Microplatelet. *Nano Lett.* **2022**, *22*, 4049−4057.
(9) Hu, F.; et al. Imaging exciton-polariton transport in $MoSe_2$ waveguides. *Nat. Photonics* **2017**, *11*, 356−360.
(10) Jahani, S.; Jacob, Z. Transparent subdiffraction optics: nanoscale light confinement without metal. *Optica* **2014**, *1*, 96.
(11) Mia, M. B.; et al. Exceptional coupling in photonic anisotropic metamaterials for extremely low waveguide crosstalk. *Optica* **2020**, *7*, 881.
(12) Ermolaev, G.; Voronin, K.; Baranov, D. G.; Kravets, V.; Tselikov, G.; Stebunov, Y.; Yakubovsky, D.; Novikov, S.; Vyshnevyy, A.; Mazitov, A.; et al. Topological phase singularities in atomically thin high-refractive-index materials. *Nat. Commun.* **2022**, *13*, 2049.
(13) Ma, W.; et al. Ghost hyperbolic surface polaritons in bulk anisotropic crystals. *Nature* **2021**, *596*, 362−366.
(14) Passler, N. C.; et al. Hyperbolic shear polaritons in low-symmetry crystals. *Nature* **2022**, *602*, 595−600.
(15) Hecht, E. *Optics, Pearson Education* **2017**, DOI: 10.1088/0022-3727/42/9/095010.
(16) Popkova, A. A.; et al. Nonlinear Exciton-Mie Coupling in Transition Metal Dichalcogenide Nanoresonators. *Laser Photon. Rev.* **2022**, *16*, 2100604.
(17) Taboada-Gutiérrez, J.; et al. Broad spectral tuning of ultra-low-loss polaritons in a van der Waals crystal by intercalation. *Nat. Mater.* **2020**, *19*, 964−968.
(18) Wu, Y.; Ou, Q.; Yin, Y.; Li, Y.; Ma, W.; Yu, W.; Liu, G.; Cui, X.; Bao, X.; Duan, J.; et al. Chemical switching of low-loss phonon polaritons in α-MoO_3 by hydrogen intercalation. *Nat. Commun.* **2020**, *11*, 2646.
(19) Li, Z.; Pestourie, R.; Park, J.-S.; Huang, Y.-W.; Johnson, S. G.; Capasso, F.; et al. Inverse design enables large-scale high-performance meta-optics reshaping virtual reality. *Nat. Commun.* **2022**, *13*, 2409.
(20) Khmelevskaia, D.; et al. Directly grown crystalline gallium phosphide on sapphire for nonlinear all-dielectric nanophotonics. *Appl. Phys. Lett.* **2021**, *118*, 201101.
(21) Tiguntseva, E. Y.; et al. Tunable Hybrid Fano Resonances in Halide Perovskite Nanoparticles. *Nano Lett.* **2018**, *18*, 5522−5529.
(22) He, X.; et al. Patterning Multicolored Microdisk Laser Arrays of Cesium Lead Halide Perovskite. *Adv. Mater.* **2017**, *29*, 1604510.
(23) Zhang, M.; et al. Growth and characterization of all-inorganic lead halide perovskite semiconductor $CsPbBr_3$ single crystals. *CrystEngComm* **2017**, *19*, 6797−6803.
(24) Rodová, M.; Knížek, K.; Nitsch, K.; Brožek, J. Phase transitions in ternary caesium lead bromide. *J. Therm. Anal. Calorim.* **2003**, *71*, 667−673.
(25) Tao, R.; et al. Halide perovskites enable polaritonic XY spin Hamiltonian at room temperature. *Nat. Mater.* **2022**, *21*, 761−766.
(26) Li, Z.; et al. High-Quality All-Inorganic Perovskite $CsPbBr_3$ Microsheet Crystals as Low-Loss Subwavelength Exciton−Polariton Waveguides. *Nano Lett.* **2021**, *21*, 1822−1830.
(27) Zhizhchenko, A. Y.; et al. Directional Lasing from Nano-patterned Halide Perovskite Nanowire. *Nano Lett.* **2021**, *21*, 10019−10025.
(28) Snaith, H. J. Perovskites: The Emergence of a New Era for Low-Cost, High-Efficiency Solar Cells. *J. Phys. Chem. Lett.* **2013**, *4*, 3623−3630.
(29) Ishteev, A.; et al. Investigation of structural and optical properties of $MAPbBr_3$ monocrystals under fast electron irradiation. *J. Mater. Chem. C* **2022**, *10*, 5821−5828.
(30) Sutherland, B. R.; Sargent, E. H. Perovskite photonic sources. *Nat. Photonics* **2016**, *10*, 295−302.
(31) Berestennikov, A. S.; Voroshilov, P. M.; Makarov, S. V.; Kivshar, Y. S. Active meta-optics and nanophotonics with halide perovskites. *Appl. Phys. Rev.* **2019**, *6*, 031307.
(32) Baranowski, M.; Plochocka, P. Excitons in Metal-Halide Perovskites. *Adv. Energy Mater.* **2020**, *10*, 1903659.
(33) Su, R.; et al. Perovskite semiconductors for room-temperature exciton-polaritonics. *Nat. Mater.* **2021**, *20*, 1315−1324.
(34) Bibi, A.; et al. Lead-free halide double perovskites: Toward stable and sustainable optoelectronic devices. *Mater. Today* **2021**, *49*, 123−144.
(35) Blancon, J.-C.; Even, J.; Stoumpos, C. C.; Kanatzidis, M. G.; Mohite, A. D. Semiconductor physics of organic−inorganic 2D halide perovskites. *Nat. Nanotechnol.* **2020**, *15*, 969−985.
(36) Ermolaev, G. A.; Yakubovsky, D. I.; Stebunov, Y. V.; Arsenin, A. V.; Volkov, V. S. Spectral ellipsometry of monolayer transition metal dichalcogenides: Analysis of excitonic peaks in dispersion. *J. Vac. Sci. Technol. B* **2020**, *38*, 014002.
(37) Liashenko, T. G.; et al. Electronic structure of $CsPbBr_{3-x}Cl_x$ perovskites: synthesis, experimental characterization, and DFT simulations. *Phys. Chem. Chem. Phys.* **2019**, *21*, 18930−18938.
(38) Toksumakov, A. N.; Ermolaev, G. A.; Slavich, A. S.; Doroshina, N. V.; Sukhanova, E. V.; Yakubovsky, D. I.; Syuy, A. V.; Novikov, S. M.; Romanov, R. I.; Markeev, A. M.; et al. High-refractive index and mechanically cleavable non-van der Waals $InGaS_3$. *npj 2D Materials and Applications* **2022**, *6*, 85.
(39) Ghosh, G. Dispersion-equation coefficients for the refractive index and birefringence of calcite and quartz crystals. *Opt. Commun.* **1999**, *163*, 95−102.
(40) Devore, J. R. Refractive Indices of Rutile and Sphalerite. *J. Opt. Soc. Am.* **1951**, *41*, 416.
(41) Zelmon, D. E.; Small, D. L.; Jundt, D. Infrared corrected Sellmeier coefficients for congruently grown lithium niobate and 5 mol% magnesium oxide − doped lithium niobate. *J. Opt. Soc. Am. B* **1997**, *14*, 3319.
(42) Dirin, D. N.; Cherniukh, I.; Yakunin, S.; Shynkarenko, Y.; Kovalenko, M. V. Solution-Grown $CsPbBr_3$ Perovskite Single Crystals for Photon Detection. *Chem. Mater.* **2016**, *28*, 8470−8474.
(43) Makarov, S.; et al. Halide-Perovskite Resonant Nanophotonics. *Adv. Opt. Mater.* **2019**, *7*, 1800784.
(44) Machnev, A. A.; et al. Modifying light−matter interactions with perovskite nanocrystals inside antiresonant photonic crystal fiber. *Photonics Res.* **2021**, *9*, 1462.
(45) Shen, W.; Chen, J.; Wu, J.; Li, X.; Zeng, H. Nonlinear Optics in Lead Halide Perovskites: Mechanisms and Applications. *ACS Photonics* **2021**, *8*, 113−124.
(46) Anikin, E. V.; Chermoshentsev, D. A.; Dyakov, S. A.; Gippius, N. A. Dyakonov-like waveguide modes in an interfacial strip waveguide. *Phys. Rev. B* **2020**, *102*, 161113.
(47) Pushkarev, A. P.; et al. A Few-Minute Synthesis of $CsPbBr_3$ Nanolasers with a High Quality Factor by Spraying at Ambient Conditions. *ACS Appl. Mater. Interfaces* **2019**, *11*, 1040−1048.
(48) Markina, D. I.; et al. Perovskite Nanowire Laser for Hydrogen Chloride Gas Sensing. *ACS Nano* **2023**, DOI: 10.1021/acsnano.2c11013.
(49) Sebastian, M.; et al. Excitonic emissions and above-band-gap luminescence in the single-crystal perovskite semiconductors $CsPbBr_3$ and $CsPbCl_3$. *Phys. Rev. B* **2015**, *92*, 235210.

https://doi.org/10.1021/acs.nanolett.2c04792
Nano Lett. XXXX, XXX, XXX−XXX